ACS OMEGA

http://pubs.acs.org/journal/acsodf

Article

N-Methyl-2-pyrrolidone as a Reaction Medium for Gold(III)-Ion Reduction and Star-like Gold Nanostructure Formation

Maleknaz Mirdamadi Esfahani,* Eric Sidney Aaron Goerlitzer, Ulrike Kunz, Nicolas Vogel, Joerg Engstler, and Annette Andrieu-Brunsen

Cite This: *ACS Omega* 2022, 7, 9484−9495

Read Online

ACCESS | Metrics & More | Article Recommendations | Supporting Information

ABSTRACT: The efficiency of a wet chemical route to synthesize gold nanostructures with tunable size and shape significantly depends on the applied solvent and the interaction of solvent molecules with other species such as gold ions. The ability of the organic solvent *N*-methyl-2-pyrrolidone (NMP) as a suitable medium for application in star-like gold nanostructure (AuNS) synthesis with a tunable morphology at ambient conditions has been investigated. The time-dependent analysis of the UV−vis absorption spectra of $Au^{III}Cl_4^-$ in a pure NMP solution illustrates the role of NMP as simultaneous complexing and reducing agents. Kinetic studies indicate that $Au^{III}Cl_4^-$ in NMP solution is reduced to $Au^{I}Cl_2^-$, with no need to use another reducing agent, any external energy sources, or solvent pretreatment. This is because Au^I species stay stable in this solution unless poly(vinylpyrrolidone) (PVP) catalyzes their disproportionation. Morphological studies by transmission electron microscopy (TEM) specify the high-yield synthesis of AuNS with monocrystalline spikes in a concentrated NMP solution by PVP. This study illustrates that the presence of seeds, as another agent to catalyze the disproportionation of Au^I species, makes it possible to synthesize AuNS in varying concentrations of PVP in this medium. The role of PVP concentration and the presence of seeds in the formation kinetics, morphology, and optical properties is systematically discussed. The results achieved through this study develop a straightforward and safe procedure for AuNS synthesis in high yield in a water-miscible organic polar solvent with tunable morphology and optical properties. Considering the high capability of NMP to dissolve various types of polymers and hydrophobic ligands, synthesizing AuNS in this solvent opens a window to a practical and easy way to fabricate gold-based nanomaterials with fascinating optical properties.

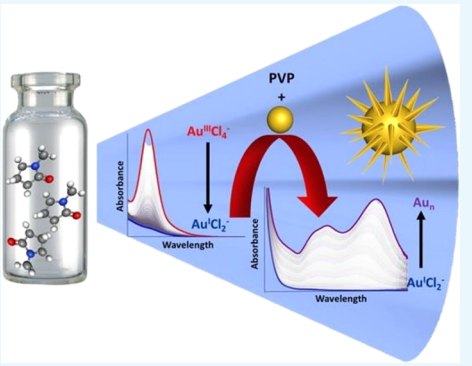

1. INTRODUTION

The application of gold-based nanomaterials has increased in various fields, such as organic solar cells,[1] electronic conductors,[2] chemical and biological sensory probes,[3] catalysis,[4−6] and medical diagnosis and treatment,[7−9] during the last few decades. These diverse applications originated from the biocompatibility[10] and exceptional optical and electrical properties of gold nanostructures. Optimizing these properties, governed by the particle shape, size, surface chemistry, aggregation state, and the surrounding medium,[11] plays a significant role in improving their performance in the aforementioned applications. The simplicity of production and the possibility to scale up are other fundamental issues in this regard. On this basis, designing and presenting new methods to synthesize gold nanoparticles (AuNPs) with a tailored morphology and properties, as well as creating a suitable condition to fabricate the gold-based nanomaterials, remains a challenge.

Among the numerous reported methods to synthesize AuNPs in a liquid phase, some protocols provide the possibility to achieve a precisely tailored size and shape, as recently summarized by a review from Liz-Marzan and colleagues.[12] AuNP synthesis in organic solvents is one of these practical chemical routes. In addition to the effective control of the size and shape of the particles, the synthesis of these particles in organic solvents creates a suitable condition to dissolve polymers and hydrophobic ligands and facilitates the fabrication of gold-based nanocomposite materials. Amide solvents, such as formamide (FMA)[13] and *N*,*N*′-dimethylformamide (DMF),[14−19] belong to this group of organic solvents. It has been demonstrated that the abovementioned amide solvents provide suitable conditions not only to dissolve and reduce gold ions but also to synthesize AuNPs with tailored optical and electrical properties through controlling the size and shape of particles. *N*-Methylpyrrolidone (NMP) is another amide solvent used in a variety of industries and applications. This aprotic organic solvent with a high boiling point and non-

Received: December 3, 2021
Accepted: February 18, 2022
Published: March 11, 2022

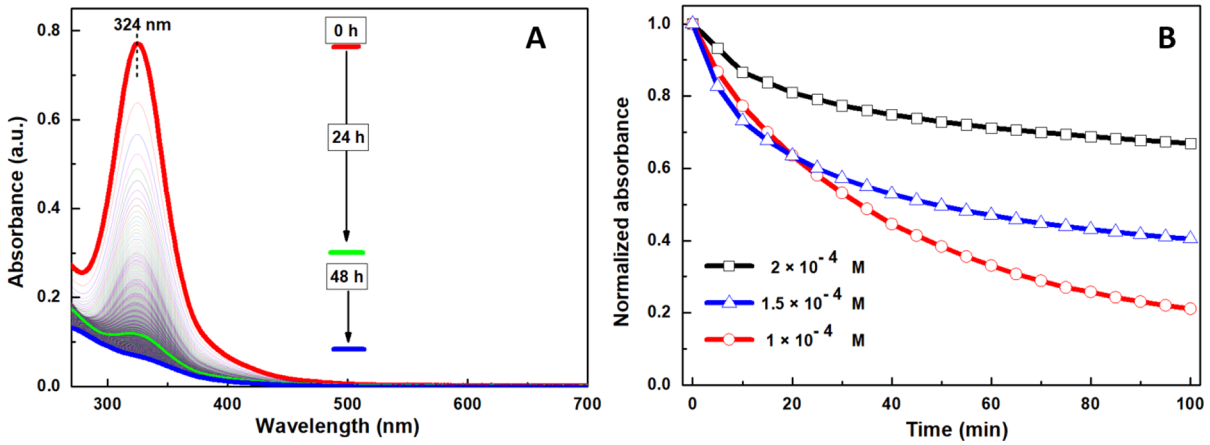

Figure 1. (A) Evaluation of UV−vis spectra of $HAuCl_4$ added at 1.5×10^{-4} M concentration to the NMP solution during 24 h (green curve) and 72 h (blue curve) (optical path: 1 cm, reference: NMP, time interval: 5 min). (B) Kinetic curves of the normalized absorbance with time registered at 324 nm during 100 min after adding the gold(III) ion complex in NMP solution.

flammable properties, as a lactam, is structurally different from other amide solvents like DMF.[20] The use of NMP, as one of the most widely used solvents in industry, considerably reduces the risk of environmental contamination due to its biodegradability.[21] NMP contains a polar heterocyclic amide group and possesses a strong polarity (μ = 4.09 D),[22] which causes the dissolution of diverse materials like polar and ionic species. At the same time, having nonpolar carbons and a large planar nonpolar region can lead to hydrophobic interactions between NMP and nonpolar molecules to form a complex.[23] This specific structure of NMP is the basis for its unique physicochemical properties,[24] and the use of NMP as a solvent, co-solvent, and complexing agent[23] in different applications such as the pharmaceutical and electronics industries.[25−28] Several studies showed that NMP could be used as potentially powerful scavengers of oxidizing agents.[29−32] Despite the various advantages of NMP, its application to create a suitable medium to synthesize metal nanoparticles has not been systematically considered. Jeon and co-workers used oxidized NMP as a solvent and a reducing agent to synthesize silver nanoparticles.[33] To produce oxidized NMP (5-hydroxy-*N*-methyl-2-pyrrolidone), they pretreated NMP through refluxing the mixture of water and NMP for 2 h at 160 °C while purging with oxygen gas. In another study, Amgoth and co-workers synthesized spherical AuNPs in a NMP solution using a strong reducing agent (sodium citrate) while the solution was being heated.[34] This study suggested that using NMP as a solvent can increase the polarity of the medium and lead to the synthesis of smaller AuNPs.[34] Yang and co-workers reported that NMP could be used as the solvent and reducing agent to synthesize palladium nanoparticles (PdNPs) dispersed on reduced graphene oxide (RGO) sheets.[35] However, they stressed that the synthesis of PdNPs would be performed by heating the NMP solution containing the Pd precursors up to 200 °C for 2 h. The mentioned studies are the first approaches of using NMP as a reducing agent to reduce metal ions. However, the effectiveness of NMP to reduce metal ions in the absence of the other reducing agents or external energy has not yet been presented yet.

This study presents NMP as a suitable medium to synthesize AuNPs with a tailored morphology and optical properties. Through kinetic studies, the capability of NMP for the reduction of gold ions has been investigated at room temperature, in an ambient atmosphere, and without the need to use external energy. The results show that by using poly(vinylpyrrolidone) (PVP) as complexing and stabilizing agents, star-like gold nanostructures (AuNSs) in a NMP solution, with a well-defined optical response, are synthesized in a straightforward process. Furthermore, the effects of the PVP concentration and the presence of preformed AuNPs on the kinetic reduction of gold ions and, consequently, on the morphology and optical response of AuNS synthesized in this organic medium are discussed based on experimental and theoretical studies. The importance of controlling the properties of AuNS is better understood by considering the various applications of this structure in different fields,[36] such as life science, sensing, thermal therapy, or drug delivery. These diverse applications are based on the optical properties and the higher enhancement factors of this structure than other morphologies for Raman spectroscopy.[37]

2. RESULTS AND DISCUSSION

To investigate the interaction between solvent molecules and other soluble components, kinetic studies of gold ion reduction were performed. Evaluation of UV−vis absorption spectra of NMP solutions containing different concentrations of hydrogen tetrachloroaurate(III) ($HAuCl_4$) (from 1 to 2×10^{-4} M) was carried out at ambient conditions. As shown in Figure 1A, $AuCl_4^-$ displays a maximum absorption at 324 nm, corresponding to a molar absorption coefficient of $\varepsilon_{324}(Au^{III})$ = 5242 ± 80 M^{-1} cm^{-1}. This absorption band at 324 nm is attributed to the ligand-to-metal charge transfer (LMCT).[38] The maximum absorption intensity of the LMCT band of the $AuCl_4^-$ ion at 324 nm in NMP solution recorded for the sample at $[HAuCl_4] = 1.5 \times 10^{-4}$ M shows decreasing maximum absorption intensity with increasing reaction time until complete disappearance after 72 h. Simultaneously, no other increased absorption band in the visible region and no sediments at the bottom of the container or stains on the glass vial are observed. These observations indicate that gold in the atomic state has not been formed upon this reaction time of 72 h. The kinetic analysis during the initial 100 min shows an exponential decay of the $Au^{III}Cl_4^-$ concentration with time (Figure 1B), indicating that the gold-ion reduction rate decreases with increasing the initial concentration of $Au^{III}Cl_4^-$.

https://doi.org/10.1021/acsomega.1c06835
ACS Omega 2022, 7, 9484−9495

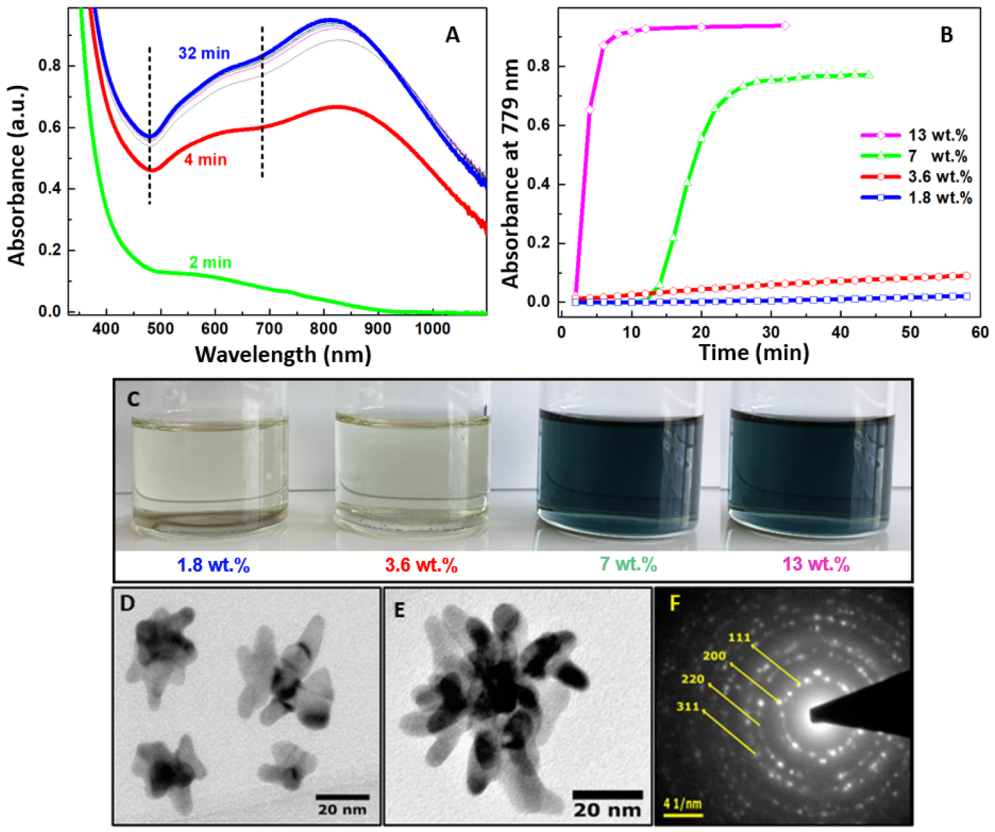

Figure 2. (A) UV−vis absorption spectra at different time intervals after adding 1.25×10^{-4} M $HAuCl_4$ to an NMP solution containing 13 wt % of PVP (optical path: 1 cm, reference: NMP, time interval: 2 min). (B) Absorbance variation at 779 nm versus the reaction time of four NMP solutions containing 1.25×10^{-4} M $HAuCl_4$ and four different concentrations (from 1.8 to 13 wt %) of PVP. (C) Photo taken 7 days after adding 1.25×10^{-4} M $HAuCl_4$ to the four glass vials containing NMP solution and 1.8, 3.6, 7, and 13 wt % of PVP (respectively, from left to right). TEM images of spiked AuNPs obtained from 10 mL of NMP solutions containing $HAuCl_4$ (1.25×10^{-4} M) and (D) 13 and (E) 7 wt % of PVP. (F) Corresponding SAED pattern for AuNS (E) showing the (111), (200), (220), and (311) reflections of gold.

It is known that NMP can be oxidized to form 5-hydroxy-*N*-methyl-2-pyrrolidone at certain conditions, such as an elevated temperature, high pressure, and in the presence of oxygen as well as metal complex catalysts like $Co(BPI)_2$, and further oxidation leads to form *N*-methyl succinimide and 2-hydroxy-*N*-methylsuccinimide in the solution.[32,39] It has also been shown that 5-hydroxy-*N*-methyl-2-pyrrolidone, produced from NMP boiling with H_2O and O_2 at 160 °C, can act as a reducing agent to reduce silver ions to silver nanoparticles.[33] The use of 2-pyrrolidinone as a promising reducing agent for the simple preparation of gold nanowires has been reported by Li and co-workers.[40] They demonstrated that peroxide species were formed during the oxidation of 2-pyrrolidinone in the presence of water and oxygen at an elevated temperature. These peroxide species, which are not stable, transform into a stronger reducing agent, 5-hydroxy-2-pyrrolidone, and this secondary alcohol can act as a reducing agent. A common point in the mentioned studies is the oxidation of the lactam groups in the presence of oxygen and in the elevated temperature to form a peroxide species in the first step and the formation of the secondary alcohol under further oxidation, which can act as the reducing agent in the presence of metal ions (Scheme S1).

Investigating the role of NMP as a reducing agent in the current study has been performed at ambient conditions with no need to use any external energy. It should be noted that all experiments have been carried out using freshly received anhydrous 99.5% NMP to make sure that the probability of the presence of NMP-oxidized species in the samples has been very low.

It is generally accepted that the $Au^{III}Cl_4^-$ photodissociation occurs due to the light absorption by the LMCT band of the $Au^{III}Cl_4^-$ ions and $Au^{II}Cl_3^-$, and chlorine radical can be formed when the electron is completely detached from chlorine.[41−43]

$$Au^{III}Cl_4^- \xrightarrow{h\upsilon} [Au^{III}Cl_4^-]^* \quad (1)$$

$$[Au^{III}Cl_4^-]^* \rightarrow Au^{II}Cl_3^- + Cl^\circ \quad (2)$$

$Au^{II}Cl_3^-$ is very unstable, and the intramolecular disproportionation reaction leads to $Au^{I}Cl_2^-$ and $Au^{III}Cl_4^-$.[44]

$$2Au^{II}Cl_3^- \rightarrow Au^{III}Cl_4^- + Au^{I}Cl_2^- \quad (3)$$

The occurrence of reactions 1−3 in the experiments is shown in Figure S1 by adding 1.5×10^{-4} M of $HAuCl_4$ in an aqueous solution and evaluating the absorption spectra of this solution during 24 h. As presented in the inset image in Figure S1, decreasing the absorption band at 288 nm and the simultaneous blue shift is attributed to the $Au^{III}Cl_4^-$ reduction. Simultaneously, the increase of the intensity of the specific shoulder below 250 nm, attributed to $Au^{II}Cl_3^-$ species, results in an isosbestic point formation at 274 nm. The disproportionation of $Au^{II}Cl_3^-$ (reaction 3) causes the balance between these complex ions to be created, and a slight decrease at 288 nm is to be observed during 24 h. In NMP solution, the

https://doi.org/10.1021/acsomega.1c06835
ACS Omega 2022, 7, 9484−9495

decay of $Au^{III}Cl_4^-$ ions is not of the first-order (Figure 1B), and no isosbestic point is observed in Figure 1A. This observation indicates that an additional reaction occurs after ligand substitution, which most probably is related to the reduction of the $Au^{III}Cl_4^-$ ions via the oxidation of the coordinated NMP molecule by the metal center. This phenomenon is similar to the reduction of $Au^{III}Cl_4^-$ ions in methanol.[45] Based on the decrease of the $Au^{III}Cl_4^-$ absorption band in this solution over time, and its disappearance after a certain time determined by the initial concentration of gold (Figure 1A), we conclude that NMP in these experiments serves as a reducing agent, which reduces $Au^{III}Cl_4^-$ to $Au^{II}Cl_3^-$ at this stage. Subsequently, $Au^{II}Cl_3^-$ disproportionates to $Au^{I}Cl_2^-$ and $Au^{III}Cl_4^-$. Reproducing $Au^{III}Cl_4^-$ ions in the reaction medium causes the gold-ion reduction rate to decrease with increasing the initial concentration of gold in NMP solutions (Figure 1B). Because no other absorption band in the UV−vis region was observed and no sediment formed at the bottom of the container, it is considered that gold clusters have not been created.[41] This indicates that $Au^{I}Cl_2^-$ is the only stable species in NMP solution after 72 h, as its absorbance between 260 and 700 nm is negligible according to the literature.[46] It is reported that Au^{I} species are frequently unstable and disproportionate to gold atoms and Au^{III} oxidation states.[47] However, depending on the nature of the ligand and the nature of the solvent, Au^{I} species can present relative stability against the disproportionation reaction.[41,48,49] This stability is a function of the reduction potential of Au^{I} species, in such a way that the polarographic reduction of Au^{I} species changes from ca. −1 V (SCE) to ca. −1.5 V (SCE) based on the type of the complexing agents.[50] Considering the previous studies regarding the effect of the ligand exchange processes on the reduction potential of gold ions,[51] the ligand exchange processes of $Au^{I}Cl_2^-$ in the presence of NMP can be considered as a reasonable factor that changes the reduction potential of Au^{I} species and creates a thermodynamical barrier to reducing $Au^{I}Cl_2^-$ into gold clusters by NMP or through a spontaneous disproportionation. This point can be mentioned in the parenthesis that creating a sustainable $Au^{I}Cl_2^-$ in NMP solution, as a widely used organic medium, is one of the remarkable points of this study due to the importance of Au^{I} chloride species as reactants and intermediates in various chemical sciences and engineering processes.[52]

To complete the $Au^{III}Cl_4^-$ reducing process and perform the last reduction step ($Au^{I} \rightarrow Au^{0}$), as well as the nucleation and growth of gold clusters, poly(vinylpyrrolidone) (PVP), was added to the NMP solution. By adding $Au^{III}Cl_4^-$ ions to an NMP solution containing 13 wt % of PVP, a shoulder/band in the visible region (around 550 nm) was recorded after 2 min (Figure 2A), and the colorless solution turned blue in less than 5 min (Figure 2C). The appearance of the localized surface plasmon resonance (LSPR) of AuNPs, as well as the color change of the solution, indicate that the reduction process of $Au^{III}Cl_4^-$ has been completed and that nucleation occurred. This LSPR band evolves over time, and a very intense band appears in the vis-NIR region after aging for 32 min (Figure 2A). The rate of this process decreased with decreasing PVP concentration (Figure 2B) so that no color change has been observed during the following hours for solutions containing a lower PVP concentration (1.8 and 3.6 wt %). However, micron-sized particles were visible at the bottom of these containers after about 1 week (Figure 2C). As shown in Figure 2A, the LSPR band of AuNPs formed in the NMP solutions containing high concentrations of PVP results from the hybridization of plasmons associated with two prominent structures. An intense absorbance band was recorded at wavelengths above 700 nm and a less intense band/shoulder between 500 and 650 nm. The same plasmon band was previously reported for branched gold nanostructures.[53−55] These studies mentioned that the weak absorption in the visible region is attributed to the plasmon resonance of the core and the dominant plasmon band above 700 nm is related to the resonance supported by the branches. Increasing the PVP concentration from 7 to 13 wt % in the growth solution caused the band at 808 nm to slightly blue shift and the band/shoulder at the visible region to become more intense (Figure S2). It has been established that variations in the morphology of particles can explain such optical changes.[56] Transmission electron microscopy (TEM) characterization revealed spiked particles, and no other shapes were observed in the sample for the nanostructures (Figure 2D,E). Comparing Figures 2D and 3F with Figures 2E and 3E clearly shows that increasing the PVP concentration in the solutions leads to the formation of smaller particles with fewer and shorter spikes. The corresponding selected area electron diffraction (SAED) pattern of AuNS shows the concentric diffraction rings with bright spots (Figure 2F), demonstrating the polycrystalline nature of these nanostructures.

To better understand how the number of spikes affects the optical properties of AuNS synthesized in NMP, the LSPR bands of spherical (Figure 3A) and spiked (Figure 3B,C) gold nanostructures were compared. This comparison shows that the absorption spectra of gold nanostructures with growing spikes on their core centers (Figure 3B,C) display LSPR bands in the NIR in addition to the green regions of the visible spectrum, as observed in spherical particles (Figure 3A). Furthermore, increasing the number of spikes causes a red shift of the maximum absorption in the NIR region. It can be concluded that the anisotropic distribution of the electromagnetic field at the tips in nonspherical Au nanostructures can facilitate the localization of electromagnetic fields in these structures. This result is consistent with the results presented for anisotropic metal nanoparticles.[57] Finite element model (FEM) simulations were performed using three different simplified models (inset images in Figure 3G) to support the experimental results. The simulated extinction cross-section spectra, obtained from the combination of absorbance and scattering spectra for all the models, show the intrinsic properties of AuNS exhibiting both longitudinal and transverse plasmon resonance corresponding to the spikes at the NIR region and the center core at the visible region, respectively (Figures S4 and 3G). Additionally, the near-field enhancement distribution maps calculated for the mentioned models at the wavelengths of the different band maxima show that the plasmon resonance confined within the spikes dominates the overall optical response over interspike interactions and dipolar oscillations confined within the central body (Figure 3H). The results obtained through these simulations (Figure 3G) are consistent with the experimental data (Figure S2) and demonstrate that increasing the number of spikes leads to increasing the intensity and the red shift of the longitudinal resonance wavelength. At the same time, the transverse resonance wavelength appears at the same position with a slightly decreased intensity. This finding is in line with previous experimental and theoretical studies regarding the AuNS optical properties.[55,58,59]

https://doi.org/10.1021/acsomega.1c06835
ACS Omega 2022, 7, 9484−9495

Scheme 1. Schematic Illustration of the Disproportionation Reaction in the Presence of PVP: Complexation of Au^I Chloride Species and the Creation of Aurophilic Interaction in the Presence of PVP in the First Step, Electron Transfer (I), and Gold Atom Formation in the Second Step (II)

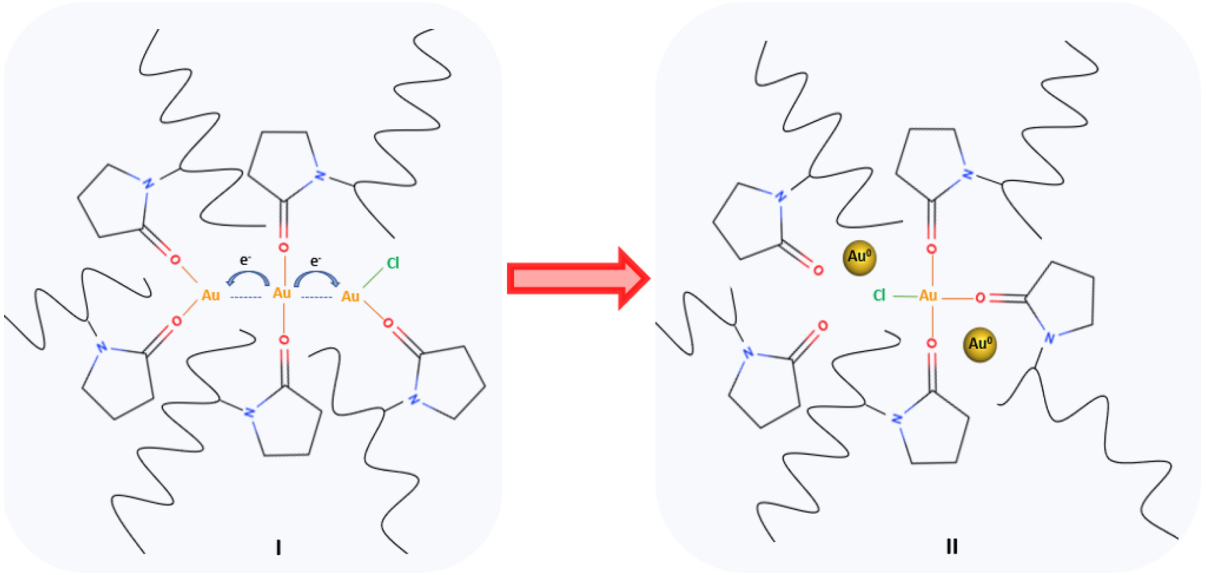

To explain the role of PVP in completing the gold-ion reduction process and the formation of gold atoms, the structure of this polymer has to be considered. A lone pair of electrons on N and O atoms of the lactam unit and its ability to generate active binding sites upon mesomerism[60] allows PVP to form charge-transfer (CT) complexes with metal ions.[61−63] On this basis, the three possible coordinations through the electrostatic interaction of amide groups of pyrrolidone rings and Au(I) chloride species are pictured in Scheme S2. The formation of gold particles in the presence of PVP indicates that these interactions can allow one to overcome the thermodynamic barrier and facilitate the Au^I species reduction into gold atoms. This effect can be explained in two ways: (I) the change of the reduction potential of Au^I species through creating new Au^I complexes,[41] (II) the increase of the possibility of exchanging electrons between neighboring Au^I species and facilitation of the disproportion reaction. The latter can be attributed to creating the right conditions to direct and improve the aurophilic interaction.[64] This hypothesis is illustrated in Scheme 1.

Thus, the last step of the gold-ion reduction and the first step of the particle construction might be performed in this condition via the reducing agents (NMP and PVP) or through the disproportionation of $Au^ICl_2^-$, based on the following reaction[47]

$$3Au^ICl_x^{1-x} \rightarrow Au^{III}Cl_y^{3-y} + 2Au^0 + (3x - y)Cl^- \quad (4)$$

Based on pulse radiolysis studies on noble metal ion reduction, nucleation, and nanoparticle growth,[49,65−67] it is known that atoms, as soon as they are formed, not only dimerize but also may associate readily with excess metal ions. Thus, the charged dimers and, in the following, oligomers will be formed on atoms as nucleation centers instead of creating new free atoms through the association/in situ reduction process.[65] Actually, these nucleation centers are reported to behave as small electrodes, and the native cluster surfaces can catalyze the gold complex-ion reduction.[41,47] The competition between the reduction of free ions and the in situ reduction of ions located on atoms and oligomers depends on the remaining concentration of free ions as well as the PVP concentration.[65]

The influence of the PVP concentration on the growth of gold structures can be justified by considering the different roles of PVP as a complexing agent, shape-directing agent, and stabilizing agent.[68] In low concentrations of PVP (1.8 and 3.6 wt %) as a complexing agent in the NMP solution, suitable conditions to create the aurophilic interaction between Au^I species are more limited. On this basis, the reduction of monovalent gold ions is more partial and consequently, nucleation centers created in these solutions will be scarce. This small amount of nucleation centers causes a decrease in the AuNP formation rate, as shown in Figure 2B. In the presence of a low amount of nucleation centers, oligomers are developed, and a dramatic growth through the adsorption and a slow reduction of Au(I) complex ions on their surfaces happens.[41] The micrometer particles precipitated at the glass vial bottom of the samples containing a low concentration of PVP (1.8 and 3.6 wt %) after one week support this claim (Figure 2C). Increasing the PVP concentration (7 and 13 wt %) not only influences the reduction kinetics and increases the AuNP formation rate (Figure 2B) but also leads to preferential growth along certain crystalline faces of the initial nuclei and consequently to the formation of spiked nanoparticles (Figure 2D,E) based on the role of PVP as a shape-directing agent. Tsuji et al.[69] proposed that PVP is responsible for shape control through adsorbing and desorbing from the different crystal facets in a preferential sequence, regardless of the molecular weight of PVP that does not have any severe effect on the size/shape of the resultant Au nanostructures. Considering the PVP action as the stabilizer agent, more and taller spikes created on native clusters are justifiable in the presence of a relatively low concentration of PVP (7 wt %). Comparing Figures 2D and 3E, which belong to Au nanostructures synthesized in the solution containing 7 wt %, with Figures 2E and 3F, which are attributed to AuNS synthesized in the solution containing a higher concentration

https://doi.org/10.1021/acsomega.1c06835
ACS Omega 2022, 7, 9484−9495

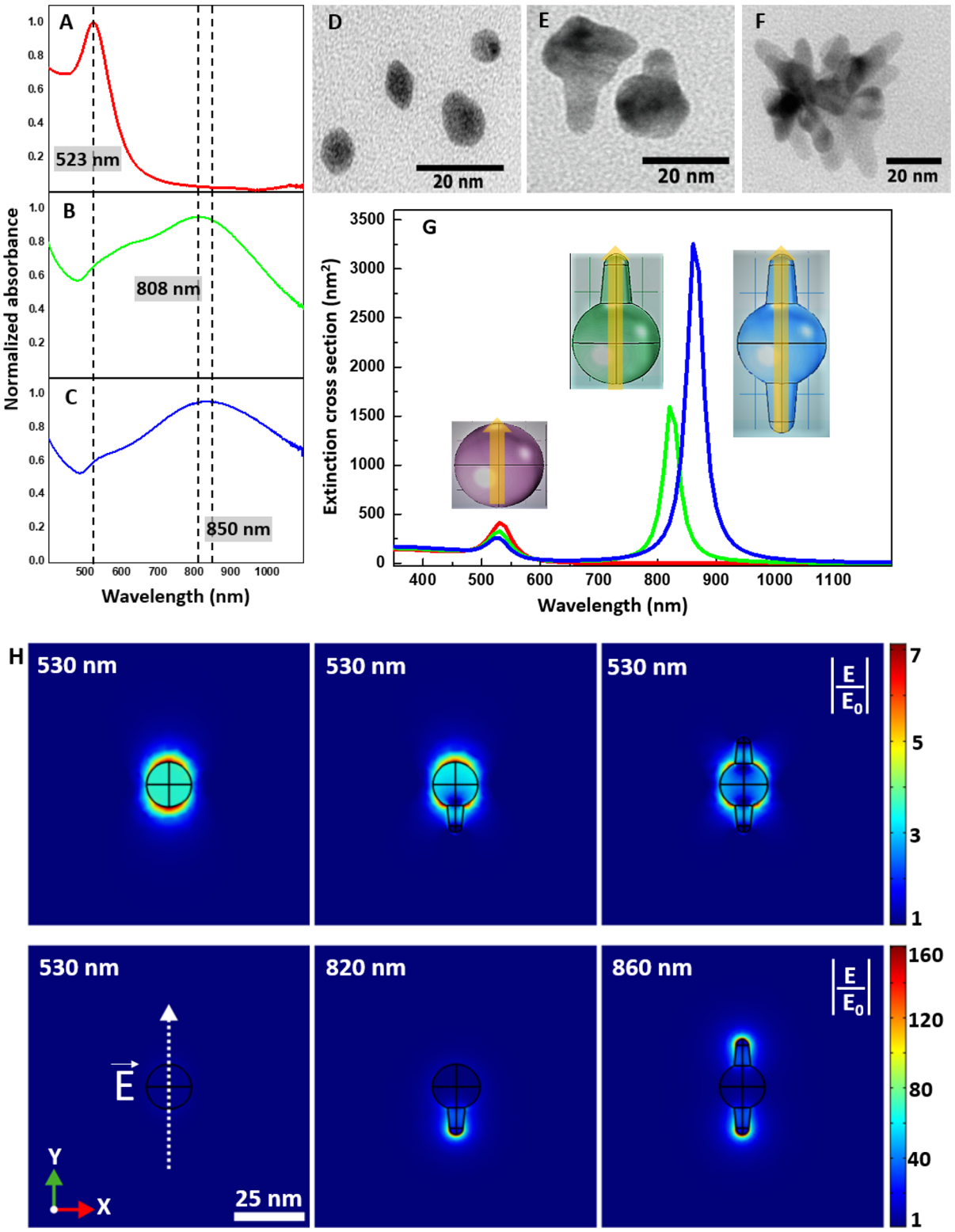

Figure 3. Absorption spectra of the colloidal solution containing (A) spherical AuNPs synthesized in an aqueous solution using a strong reducing agent ($NaBH_4$) and stabilized by PVP (3.6 wt %), (B) AuNS synthesized in an NMP solution containing a high concentration of PVP (13 wt %), and (C) AuNS synthesized in an NMP solution containing a low concentration of PVP (7 wt %). The same concentration of $HAuCl_4$ (1.25×10^{-4} M) was used in all samples. (D,E,F) TEM images of gold nanostructures synthesized in solutions (A−C), respectively. (G) Simulated extinction cross-section spectra as a function of wavelength for the AuNP targets shown in the inset images and considering the electric field polarization along longitudinal axis (LA). (H) Calculated near-field enhancement maps for the AuNP targets at wavelengths of band maxima (see labels) for polarized light along the LA and considering the dimensions presented in Figure S3.

of PVP (13 wt %), shows the effect of the stabilizer agent concentration on the size and form of AuNS.

To investigate the effect of the presence of the seeds on the reduction kinetics of gold complex ion and gold nanostructure

https://doi.org/10.1021/acsomega.1c06835
ACS Omega 2022, 7, 9484−9495

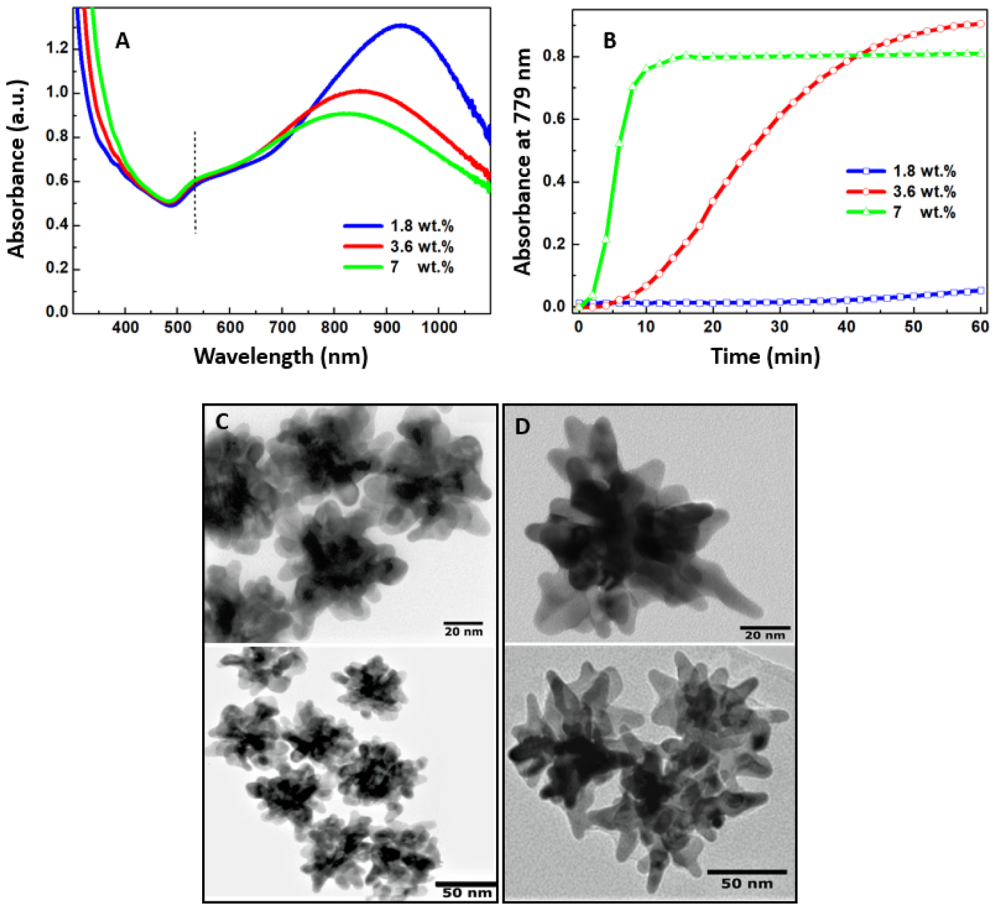

Figure 4. (A) Vis-NIR spectra of AuNPs synthesized under the same experimental conditions by adding 1.25×10^{-4} M of $HAuCl_4$ to the NMP solution containing 1.8, 3.6, and 7 wt % of PVP after aging for 24 h (optical path: 1 cm, reference: NMP, the dashed line at 540 nm is attributed to dipolar resonances localized at the central core of the particles). (B) Absorbance variation at 779 nm versus the reaction time for the three NMP solutions containing 10 μL of seed solution and different PVP concentrations (1.8, 3.6, and 7 wt %) and 1.25×10^{-4} M $HAuCl_4$. TEM images of AuNS synthesized in 10 mL of NMP solutions containing preformed seeds, $HAuCl_4$ (1.25×10^{-4} M), and (C) 7 wt % and (D) 1.8 wt % of PVP.

formation, PVP-capped AuNPs of 5−6 nm were added as nanoparticle seeds to the growth solution containing the same concentrations of gold ions and the different amounts of PVP. TEM images of the preformed seeds are shown in Figures 3D and S8, and the particle size distribution is presented in the inset image of Figure S8.

In the presence of seed particles in the growth NMP solution, containing 7 wt % of PVP, the absorbance at 779 nm, attributed to the formation of AuNS, significantly increases in the early minutes after adding gold complex ions into the solution (Figure S5). In comparison, no absorbance increase is observed during the first 12 min for the solution containing the same concentration of PVP in the absence of seeds. However, no significant difference in the formation kinetics of AuNS is observed between these two solutions after 12 min. This effect could be related to the formation of native clusters in the growth solution lacking seeds. Comparing TEM images of AuNPs synthesized in the presence (Figure 4C) and the absence (Figures 2E and 3F) of seeds in the growth solutions demonstrates that the diameter of nanostructures increases to some extent without significantly affecting the morphology of particles in the presence of seeds. This effect can be attributed to the adsorption and reduction of the gold complex ions on the seeds' surfaces acting as small electrodes, as previously mentioned. The effect of the presence of the seeds in the NMP growth solution containing a lower concentration of PVP (1.8 wt %) is more pronounced. In this case, gold nanostructures (Figure 4D) are synthesized instead of micrometer particles precipitated in the absence of seeds (Figure 2C). Evaluating the absorption spectra of this solution shows that the band/shoulder in the UV region (around 328 nm) completely disappeared during the initial 14 min, corresponding to the reduction of $Au^{III}Cl_4^-$ to $Au^{I}Cl_2$ (Figure S6). After a reaction time of 14 min, the plasmon absorption band appears and grows in the vis-NIR region while showing a red shift (inset image in Figure S6). This red spectral shifting is accompanied by a further increase in the absorption intensity of the hybridized LSPR band in the NIR region compared to the visible region. Thus, a very intense absorbance band centered around 928 nm along with a less intense band/shoulder around 540 nm was observed for this sample after 24 h (Figure 4A, blue curve). A similar form of hybridized LSPR bands with the same absorbance intensity in the visible region (around 540 nm) has been recorded for the solutions containing the higher concentration of PVP (3.6 and 7 wt %) (Figure 4A, red and green curves, respectively). However, this difference in the PVP concentration causes a significant difference in the absorbance as well as a red shift of the major band in the NIR region. TEM images of Au nanostructures synthesized in the solutions containing the most (7 wt %) and the least (1.8 wt %) amount of PVP show that the nanostructures prepared in both solutions resemble a star-like assembly with all rays

https://doi.org/10.1021/acsomega.1c06835
ACS Omega 2022, 7, 9484−9495

grown radially outward from a common center (Figures 4C,D respectively). TEM images also demonstrate the high yield AuNS synthesis in an NMP medium so that no other shapes were found through this analysis (Figure 5C). The optical

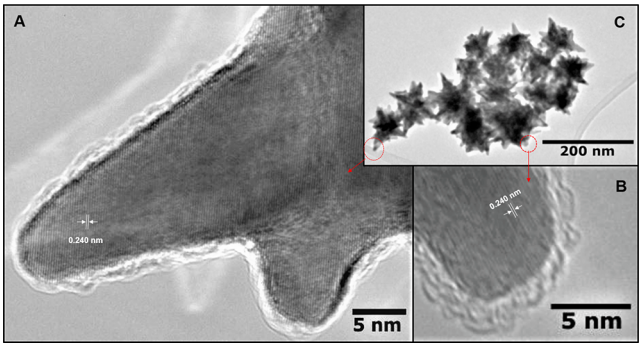

Figure 5. HRTEM images of two individual spikes in the structure of AuNS synthesized in10 mL of NMP solutions containing $HAuCl_4$ (1.25×10^{-4} M) 1.8 wt % of PVP and 10 μL of seed solution (A,B). TEM image with the lower magnification of AuNS synthesized in the same solution (C).

response of these structures (Figure 4A) is in accordance with the simulated spectra presented in Figure 3G. Comparing the formation kinetics of AuNPs in the presence of the preformed AuNP seeds (Figure 4B) and the absence of these particles (Figure 2B) in growth solutions indicates that seeds have a more significant effect in intensifying the reduction of gold complex ions in the solutions containing a low concentration of PVP that face the restriction of native clusters and nucleation centers. In other words, by adding Au preformed seeds in these solutions, gold complex ions can find more substrates to act as catalysts to adsorb and reduce on their surfaces.[47] This factor, along with the role of PVP as a reducing agent,[68] control the kinetics of the reduction of gold complex ions and the formation of AuNS. This difference in the reduction kinetics of gold complex ions along with the critical role of PVP in the preferential growth of particles along various crystal faces through adsorption/desorption sequential processes[69] cause the synthesis of AuNS with different sizes and form spikes in these solutions (Figure 4C,D). However, in addition to these two effective factors, two other factors also play an important role in controlling the shape and consequently the absorption band. The role of PVP as a stabilizing agent that controls the growth of particles,[68] and also its role as a complexing agent that affects the intra- and interchain aurophilic interactions.[64] Together, these factors cause the spikes to grow more in lower PVP concentrations, and the taller and sharper spikes form in the solution containing 1.8 wt % of PVP. Figure 4D in two different magnifications shows the formation of the taller and sharper spikes on the central core in the solution containing a lower concentration of PVP in comparison to petal-like spikes formed in the solution containing a higher concentration of PVP (Figure 4C). Because no significant difference between the number of spikes in these two samples is observed, changing the absorption intensity and red shifting the main longitudinal resonance, as presented in Figure 4A, might be attributed to the difference in the form of spikes.

High-resolution transmission electron microscopy (HRTEM) images demonstrate that gold atoms are arranged in parallel planes and form individual spikes with single-crystalline nature surrounded by amorphous PVP layers (Figure 5A,B). The lattice fringe spacing shown in the image is 0.240 nm, which corresponds to the (111) facet of the crystal plane of the gold cubic phase.[70] These HRTEM images provide reasonable evidence to justify the hypothesis of the reduction of Au^I species following the creation of the aurophilic interaction in the presence of PVP, as previously mentioned and shown in Scheme 1.

An overview of the different sizes and forms of AuNS synthesized with high yield in NMP solutions through this study is illustrated in Figure S7. These TEM images well show the ability of the presented method to synthesize AuNS with the desired morphology.

3. CONCLUSIONS

NMP, with no need for any pretreatment processes or any external energy sources, can reduce $Au^{III}Cl_4^-$ to $Au^ICl_2^-$ in an ambient temperature and pressure. Given that $Au^ICl_2^-$ are important reactants and intermediates in various processes across the chemical sciences and engineering, this study provides a way to form stable Au^Ichloride species in the organic medium NMP. In the presence of PVP, a suitable condition is created for Au^I species reduction and Au atom formation. These clusters yielded by the coalescence of these atoms behave as small electrodes and act as growth nuclei. Thus, the rate of AuNP formation is a function of the prevalence of these nucleation centers, whether in the form of native clusters or the preformed AuNP seeds. At the same time, the morphology of AuNSs, which are synthesized in the NMP/PVP mixture solution with high yield, also depends on the reduction kinetics of gold ions, which can be controlled by the number of nucleation centers as well as the concentration of PVP. Based on the dependence of AuNS optical properties to their size and shape, this research presents a simple, safe, and targeted method to synthesize these structures with the desired optical properties by controlling the reduction kinetics of gold complex ions. Considering a variety of AuNS applications in different fields due to their exceptional optical properties, the presented method can be applied in various fields. Based on the strong sensitivity of the plasmon resonance to the local dielectric environment, the synthesis of AuNSs in NMP as a widely used organic solvent is another significant point of this research. On the other hand, the synthesis of AuNS with an amphiphilic nature in an organic polar solvent creates a suitable condition for labeling their surfaces with different functional groups such as organic molecules or different hydrophobic ligands. Thus, synthesized AuNSs in this medium are envisioned to widen the applied potential of these nanostructures at various conditions. This research is in progress to create new nucleation agents and better specify the role of the aurophilic interaction in the single-crystalline nature of gold nanostructures in this medium.

4. EXPERIMENTAL SECTION

4.1. Chemicals. Tetrachloroaurate trihydrate ($HAuCl_4 \cdot 3H_2O$, 99.99%) was used as the precursor of AuNPs). *N*-Methyl-2-pyrrolidone (NMP, anhydrous, 99.5%) was used as both a solvent and reducing agent. Polyvinylpyrrolidone (PVP10, 10,000 g/mol) was both a complexing and stabilizing agent. All these chemicals were purchased from Sigma-Aldrich and used without further purification. Ultrapure water (MilliQ,

https://doi.org/10.1021/acsomega.1c06835
ACS Omega 2022, 7, 9484−9495

18.2 MΩ cm) was used as a solvent to prepare the tetrachloroaurate stocked solution (0.2 M).

4.2. Nanoparticle Preparation and Sample Handling. Studying the gold ion reduction and AuNP formation which took place by the simple addition of an appropriate amount of tetrachloroaurate-stocked aqueous solution (0.2 M) to a 30 mL glass vial containing 10 mL of the corresponding solutions (the chemical composition of each solution is listed in its place). This addition was performed, taking all necessary precautions to avoid the degradation of the micropipette plastic tips by NMP. The glass vials were closed with plastic stoppers. Due to the low vapor pressure of NMP (0.342 mm Hg at 25 °C),[71] there was no concern about the impact of NMP vapor on plastic stoppers. All the chemical reagents were mixed gently, and no vigorous stirring was required. In these experiments, PVP was entirely resolved at room temperature in pure NMP and subsequently, the gold ion solution was added.

Gold seeds of 5−6 nm (inset image in Figure S8) were prepared as previously reported.[72] Briefly, 6 μL of aqueous solution of 0.2 M $HAuCl_4$ was added to 10 mL of a PVP10 solution in H_2O containing 3.6 wt % of PVP. Next, 1 mL of a freshly prepared 0.5 M $NaBH_4$ solution was quickly injected under vigorous stirring. The colloidal solution was stirred for 1 h at room temperature. The seed was not used until 24 h after preparation to allow the complete $NaBH_4$ decomposition and avoid further nucleation. Figure S8 shows the TEM image and the particle size distribution of PVP-capped AuNPs used as seeds.

4.3. Characterization Techniques. A Cary 60 UV−vis spectrometer (Agilent Technologies, CA, USA), run by Cary WinUV program software version 5.0.0.999, was used to record the UV−vis−NIR spectra in 1 cm quartz cuvettes at a scan rate of 600 nm min^{-1} over the range 250−1100 nm. For this aim, first, a background correction was performed using a reference solution and measuring the amount of light that strikes the detector in the range of defined wavelengths (the type of reference solutions have been indicated in its place based on the type of sample). Then, these values were stored as the background scan in memory to calculate accurate absorbance values for each sample. All assays were performed at room temperature and in an ambient atmosphere.

AuNPs have been characterized by TEM. TEM studies have been performed with a Philips CM20 instrument, operated at 200 kV. First, the colloidal dispersion was centrifuged at 6000 rpm for 30 min to remove the organic solvent. Next, the colorless supernatant was replaced by pure water, and then AuNPs were dispersed by sonication for 10 min. Finally, a drop of the dispersed AuNPs in aqueous solution was deposited on a standard carbon-coated TEM copper grid. Bright-field images provided by TEM, along with the corresponding SAED pattern, have presented details regarding morphologic and crystallographic information of synthesized AuNPs. In addition, HRTEM images were taken at 200 kV using a TECNAI G2 F20 from FEI.

4.4. Optical Modeling. FEM simulations using the commercial software COMSOL Multiphysics have been carried out to quantify the absorption, scattering, and extinction cross-section spectra of individual AuNPs. The single objects were surrounded by perfectly matched layers (PMLs) in all directions. The geometrical models, as represented in Figure S3 and the inset images in Figure 3G, have been graphically depicted considering the AuNP morphology as presented in Figure 3E. Simplified models have been considered for the calculations consisting of a central sphere with either none, one, or two pseudoconical caps located symmetrically opposite to the central core. The refractive index of the surrounding medium was chosen as 1.5 without dispersion. The permittivity of the gold was taken from literature.[73] The illumination was a monochromatic plane wave, which was linearly polarized either along the *X*-axis (Transverse Axis, TA) or the *Y*-axis (Longitudinal Axis, LA). Light propagation was perpendicular to the structures along the *Z*-axis. Maxwell's equations were solved in the wavelength ranges of 350 and 1200 nm in 10 nm steps.

■ ASSOCIATED CONTENT

Supporting Information

The Supporting Information is available free of charge at https://pubs.acs.org/doi/10.1021/acsomega.1c06835.

> Mechanism of gold ion reduction by 2-pyrrolidinone in the presence of H_2O and O_2; kinetic study of gold ion reduction in NMP and aqueous solutions; investigation of the effect of PVP concentration and seed presence in LSPR and morphology of AuNS synthesized in NMP solution; simplified model considered for the optical spectra and near-field enhancement map calculations; scattering, absorption, and extinction cross-section spectra simulated as a function of wavelength for the AuNP targets; scheme of PVP and Au^I species coordination; and TEM images of AuNPs synthesized and used as seeds (PDF)

■ AUTHOR INFORMATION

Corresponding Author

Maleknaz Mirdamadi Esfahani − *Ernst-Berl Institut für Technische und Makromolekulare Chemie, Technische Universität Darmstadt, 64287 Darmstadt, Germany;* orcid.org/0000-0002-9077-619X; Email: mirdamadimaleknaz@gmail.com

Authors

Eric Sidney Aaron Goerlitzer − *Institute of Particle Technology, Friedrich-Alexander University Erlangen-Nürnberg, D-91058 Erlangen, Germany;* orcid.org/0000-0003-4088-929X

Ulrike Kunz − *Department of Materials and Earth Sciences, Physical Metallurgy Group, Technische Universität Darmstadt, 64287 Darmstadt, Germany*

Nicolas Vogel − *Institute of Particle Technology, Friedrich-Alexander University Erlangen-Nürnberg, D-91058 Erlangen, Germany;* orcid.org/0000-0002-9831-6905

Joerg Engstler − *Eduard-Zintl-Institut für Anorganische und Physikalische Chemie, Technische Universität Darmstadt, 64287 Darmstadt, Germany*

Annette Andrieu-Brunsen − *Ernst-Berl Institut für Technische und Makromolekulare Chemie, Technische Universität Darmstadt, 64287 Darmstadt, Germany;* orcid.org/0000-0002-3850-3047

Complete contact information is available at: https://pubs.acs.org/10.1021/acsomega.1c06835

Author Contributions

All authors have given to the final version of the manuscript.

https://doi.org/10.1021/acsomega.1c06835
ACS Omega 2022, 7, 9484−9495

Funding

This study has been performed in line with the Re-entry Scholarship offered by the Gender Equality Office of the Technical University (TU) Darmstadt.

Notes

The authors declare no competing financial interest.

■ ACKNOWLEDGMENTS

The authors are thankful for fruitful discussions with Prof. Mehran Mostafavi, Professor of Physical Chemistry at Paris-Sud University, and Raheleh Pardehkhorram, the postdoctoral researcher in the research group Macromolecular Chemistry - Smart Membranes at TU-Darmstadt, for collaborating on setting the manuscript. The authors also thank the Institute of Macromolecular and Paper Chemistry at the TU Darmstadt in Germany and the Department of Chemistry at the Amirkabir University of Technology in Iran to access the facilities needed for doing this study. Furthermore, the financial support of the Gender Equality Office of the Technical University (TU) Darmstadt is appreciated. We acknowledge support by the Deutsche Forschungsgemeinschaft (DFG − German Research Foundation) and the Open Access Publishing Fund of Technische Universität Darmstadt.

■ ABBREVIATIONS

NMP, *N*-methyl-2-pyrrolidone; PVP, poly(vinylpyrrolidone); DMF, *N*,*N*-dimethylformamide; FMA, formamide; $HAuCl_4$, hydrogen tetrachloroaurate(III); $NaBH_4$, sodium borohydride; AuNPs, gold nanoparticles; AuNSs, star-like gold nanostructures; PdNPs, palladium nanoparticles; LMCT, ligand-to-metal charge transfer; LSPR, localized surface plasmon resonance; vis, visible; NIR, near-infrared; TA, transverse axis; LA, longitudinal axis; TEM, transmission electron microscopy; HRTEM, high-resolution transmission electron microscopy; SAED, selected area electron diffraction; CT, charge transfer; FEM, finite element model; PML, perfectly matched layers

■ REFERENCES

(1) Notarianni, M.; Vernon, K.; Chou, A.; Aljada, M.; Liu, J.; Motta, N. Plasmonic effect of gold nanoparticles in organic solar cells. *Sol. Energy* **2014**, *106*, 23−37.

(2) Huang, D.; Liao, F.; Molesa, S.; Redinger, D.; Subramanian, V. Plastic-compatible low resistance printable gold nanoparticle conductors for flexible electronics. *JES* **2003**, *150*, G412.

(3) Saha, K.; Agasti, S. S.; Kim, C.; Li, X.; Rotello, V. M. Gold Nanoparticles in Chemical and Biological Sensing. *Chem. Rev.* **2012**, *112*, 2739−2779.

(4) Thompson, D. T. Using gold nanoparticles for catalysis. *Nano Today* **2007**, *2*, 40−43.

(5) Hashmi, A. S. K.; Hutchings, G. J. Gold Catalysis. *Angew. Chem., Int. Ed.* **2006**, *45*, 7896−7936.

(6) Hashmi, A. S. K. Sub-nanosized gold catalysts. *Science* **2012**, *338*, 1434.

(7) Wu, Y.; Ali, M. R. K.; Chen, K.; Fang, N.; El-Sayed, M. A. Gold nanoparticles in biological optical imaging. *Nano Today* **2019**, *24*, 120.

(8) Ghosh, P.; Han, G.; De, M.; Kim, C.; Rotello, V. Gold nanoparticles in delivery applications. *Adv. Drug Delivery Rev.* **2008**, *60*, 1307.

(9) Yang, W.; Liang, H.; Ma, S.; Wang, D.; Huang, J. Gold nanoparticle based photothermal therapy: Development and application for effective cancer treatment. *Sustainable Mater. Technol.* **2019**, *22*, No. e00109.

(10) Freese, C.; Gibson, M. I.; Klok, H.-A.; Unger, R. E.; Kirkpatrick, C. J. Size- and Coating-Dependent Uptake of Polymer-Coated Gold Nanoparticles in Primary Human Dermal Microvascular Endothelial Cells. *Biomacromolecules* **2012**, *13*, 1533−1543.

(11) Kelly, K. L.; Coronado, E.; Zhao, L. L.; Schatz, G. C. The Optical Properties of Metal Nanoparticles: The Influence of Size, Shape, and Dielectric Environment. *J. Phys. Chem. B* **2003**, *107*, 668−677.

(12) Grzelczak, M.; Pérez-Juste, J.; Mulvaney, P.; Liz-Marzán, L. M. Shape Control in Gold Nanoparticle Synthesis. *Colloidal Synthesis of Plasmonic Nanometals*; Jenny Stanford Publishing, 2020; pp 197−220.

(13) Han, M. Y.; Quek, C. H.; Huang, W.; Chew, C. H.; Gan, L. M. A Simple and Effective Chemical Route for the Preparation of Uniform Nonaqueous Gold Colloids. *Chem. Mater.* **1999**, *11*, 1144−1147.

(14) Pastoriza-Santos, I.; Liz-Marzán, L. M. N,N-Dimethylformamide as a Reaction Medium for Metal Nanoparticle Synthesis. *Adv. Funct. Mater.* **2009**, *19*, 679−688.

(15) Chen, Y.; Gu, X.; Nie, C.-G.; Jiang, Z.-Y.; Xie, Z.-X.; Lin, C.-J. Shape controlled growth of gold nanoparticles by a solution synthesis. *ChemComm* **2005**, 4181−4183.

(16) Pastoriza-Santos, I.; Liz-Marzán, L. M. Formation of PVP-Protected Metal Nanoparticles in DMF. *Langmuir* **2002**, *18*, 2888−2894.

(17) Kawasaki, H.; Yamamoto, H.; Fujimori, H.; Arakawa, R.; Iwasaki, Y.; Inada, M. Stability of the DMF-Protected Au Nanoclusters: Photochemical, Dispersion, and Thermal Properties. *Langmuir* **2010**, *26*, 5926−5933.

(18) Liu, X.; Li, C.; Xu, J.; Lv, J.; Zhu, M.; Guo, Y.; Cui, S.; Liu, H.; Wang, S.; Li, Y. Surfactant-Free Synthesis and Functionalization of Highly Fluorescent Gold Quantum Dots. *J. Phys. Chem. C* **2008**, *112*, 10778−10783.

(19) Barbosa, S.; Agrawal, A.; Rodríguez-Lorenzo, L.; Pastoriza-Santos, I.; Alvarez-Puebla, R. A.; Kornowski, A.; Weller, H.; Liz-Marzán, L. M. Tuning Size and Sensing Properties in Colloidal Gold Nanostars. *Langmuir* **2010**, *26*, 14943−14950.

(20) Sherwood, J.; Farmer, T. J.; Clark, J. H. Catalyst: Possible Consequences of the N-Methyl Pyrrolidone REACH Restriction. *Chem* **2018**, *4*, 2010.

(21) Chow, S. T.; Ng, T. L. The biodegradation of N-methyl-2-pyrrolidone in water by sewage bacteria. *Water Res* **1983**, *17*, 117.

(22) Fischer, E. The electric moment of 1-methylpyrrolid-2-one. *J. Chem. Soc.* **1955**, 1382−1383.

(23) Sanghvi, R.; Narazaki, R.; Machatha, S. G.; Yalkowsky, S. H. Solubility improvement of drugs using N-methyl pyrrolidone. *AAPS PharmSciTech* **2008**, *9*, 366−376.

(24) Basma, N. S.; Headen, T. F.; Shaffer, M. S. P.; Skipper, N. T.; Howard, C. A. Local Structure and Polar Order in Liquid N-Methyl-2-pyrrolidone (NMP). *J. Phys. Chem. B* **2018**, *122*, 8963−8971.

(25) Jouyban, A.; Fakhree, M. A. A.; Shayanfar, A. Review of Pharmaceutical Applications of N-Methyl-2-Pyrrolidone. *J. Pharm. Pharm. Sci.* **2010**, *13*, 524.

(26) Roche-Molina, M.; Hardwick, B.; Sanchez-Ramos, C.; Sanz-Rosa, D.; Gewert, D.; Cruz, F. M.; Gonzalez-Guerra, A.; Andres, V.; Palma, J. A.; Ibanez, B.; Mckenzie, G.; Bernal, J. A. The pharmaceutical solvent N-methyl-2-pyrollidone (NMP) attenuates inflammation through Krüppel-like factor 2 activation to reduce atherogenesis. *Sci. Rep.* **2020**, *10*, 11636.

(27) Beaulieu, H. J.; Schmerber, K. R. M-Pyrol (NMP) Use in the Microelectronics Industry. *Appl. Occup. Environ. Hyg.* **1991**, *6*, 874−880.

(28) Gómez, H.; Ram, M. K.; Alvi, F.; Villalba, P.; Stefanakos, E.; Kumar, A. Graphene-conducting polymer nanocomposite as novel electrode for supercapacitors. *J. Power Sources* **2011**, *196*, 4102.

(29) Poulain, L.; Monod, A.; Wortham, H. Development of a new on-line mass spectrometer to study the reactivity of soluble organic compounds in the aqueous phase under tropospheric conditions: Application to OH-oxidation of N-methylpyrrolidone. *J. Photochem. Photobiol., A* **2007**, *187*, 10.

(30) Hua, G.; Zhang, Q.; McManus, D.; Slawin, A. M. Z.; Woollins, J. D. Improvement of the Fe-NTA sulfur recovery system by the

https://doi.org/10.1021/acsomega.1c06835
ACS Omega 2022, 7, 9484−9495

addition of a hydroxyl radical scavenger. *Phosphorus, Sulfur Silicon Relat. Elem.* **2007**, *182*, 181−198.
(31) Lennon, G.; Willox, S.; Ramdas, R.; Funston, S. J.; Klun, M.; Pieh, R.; Fairlie, S.; Dobbin, S.; Cobice, D. F. Assessing the Oxidative Degradation of N-Methylpyrrolidone (NMP) in Microelectronic Fabrication Processes by Using a Multiplatform Analytical Approach. *J. Anal. Methods Chem.* **2020**, *2020*, 8265054.
(32) Drago, R. S.; Riley, R. Oxidation of N-alkyl amides to novel hydroperoxides by dioxygen. *J. Am. Chem. Soc.* **1990**, *112*, 215−218.
(33) Jeon, S.-H.; Xu, P.; Mack, N. H.; Chiang, L. Y.; Brown, L.; Wang, H.-L. Understanding and Controlled Growth of Silver Nanoparticles Using Oxidized N-Methyl-pyrrolidone as a Reducing Agent. *J. Phys. Chem. C* **2010**, *114*, 36−40.
(34) Amgoth, C.; Singh, A.; Santhosh, R.; Yumnam, S.; Mangla, P.; Karthik, R.; Guping, T.; Banavoth, M. Solvent assisted size effect on AuNPs and significant inhibition on K562 cells. *RSC Adv.* **2019**, *9*, 33931−33940.
(35) Yang, S.; Dong, J.; Yao, Z.; Shen, C.; Shi, X.; Tian, Y.; Lin, S.; Zhang, X. One-Pot Synthesis of Graphene-Supported Monodisperse Pd Nanoparticles as Catalyst for Formic Acid Electro-oxidation. *Sci. Rep.* **2014**, *4*, 4501.
(36) Pallavicini, P.; Cabrini, E.; Borzenkov, M.; Sironi, L.; Chirico, G. Applications of Gold Nanostars: Nanosensing, Thermal Therapy, Delivery Systems. *Gold Nanostars; SpringerBriefs in Materials*; Springer: Cham, 2015; pp 43−59.
(37) Hao, F.; Nehl, C. L.; Hafner, J. H.; Nordlander, P. Plasmon Resonances of a Gold Nanostar. *Nano Lett.* **2007**, *7*, 729−732.
(38) Isci, H.; Mason, W. R. Ligand-to-metal charge-transfer spectra of tetrahaloaurate(III) and trans-dicyanodihaloaurate(III) ions. *Inorg. Chem.* **1983**, *22*, 2266−2272.
(39) Campbell, H. L.; Striebig, B. A. Evaluation of N-Methylpyrrolidone and Its Oxidative Products Toxicity Utilizing the Microtox Assay. *Environ. Sci. Technol.* **1999**, *33*, 1926−1930.
(40) Li, C. C.; Chen, L. B.; Li, Q. H.; Wang, T. H. Seed-free, aqueous synthesis of gold nanowires. *CrystEngComm* **2012**, *14*, 7549−7551.
(41) Gachard, E.; Remita, H.; Khatouri, J.; Keita, B.; Nadjo, L.; Belloni, a. J. Radiation-induced and chemical formation of gold clusters. *New J. Chem.* **1998**, *22*, 1257−1265.
(42) Henglein, A. Radiolytic Preparation of Ultrafine Colloidal Gold Particles in Aqueous Solution: Optical Spectrum, Controlled Growth, and Some Chemical Reactions. *Langmuir* **1999**, *15*, 6738−6744.
(43) Eustis, S.; El-Sayed, M. A. Molecular Mechanism of the Photochemical Generation of Gold Nanoparticles in Ethylene Glycol: Support for the Disproportionation Mechanism. *J. Phys. Chem. B* **2006**, *110*, 14014−14019.
(44) Dey, G. R.; El Omar, A. K.; Jacob, J. A.; Mostafavi, M.; Belloni, J. Mechanism of Trivalent Gold Reduction and Reactivity of Transient Divalent and Monovalent Gold Ions Studied by Gamma and Pulse Radiolysis. *J. Phys. Chem. A* **2011**, *115*, 383−391.
(45) Quinn, M.; Mills, G. Surface-Mediated Formation of Gold Particles in Basic Methanol. *J. Phys. Chem.* **1994**, *98*, 9840−9844.
(46) Lingane, J. J. Standard potentials of half-reactions involving + 1 and + 3 gold in chloride medium: Equilibrium constant of the reaction AuCl4− + 2Au + 2Cl− = 3AuCl2−. *J. Electroanal. Chem.* **1962**, *4*, 332.
(47) Gammons, C. H.; Yu, Y.; Williams-Jones, A. E. The disproportionation of gold(I) chloride complexes at 25 to 200°C. *Geochim. Cosmochim. Acta* **1997**, *61*, 1971.
(48) Koelle, U.; Laguna, A. Electrochemistry of Au-complexes. *Inorg. Chim. Acta* **1999**, *290*, 44.
(49) Mosseri, S.; Henglein, A.; Janata, E. Reduction of dicyanoaurate(I) in aqueous solution: formation of nonmetallic clusters and colloidal gold. *J. Phys. Chem.* **1989**, *93*, 6791−6795.
(50) Bard, A. J.; Ketelaar, J. A. A. Encyclopedia of Electrochemistry of the Elements. *J. Electrochem. Soc.* **1974**, *121*, 212C.
(51) Simon, S.; Clarke, O. J. R.; Burgess, I. J. On the ligand exchange, redox, and disproportionation processes of tetrachloroaurate in the presence of a pyridine derivative. *Electrochim. Acta* **2020**, *363*, 137213.
(52) Chang, S.-Y.; Uehara, A.; Booth, S. G.; Ignatyev, K.; Mosselmans, J. F. W.; Dryfe, R. A. W.; Schroeder, S. L. M. Structure and bonding in Au (I) chloride species: a critical examination of X-ray absorption spectroscopy (XAS) data. *RSC Adv.* **2015**, *5*, 6912−6918.
(53) Hao, E.; Bailey, R. C.; Schatz, G. C.; Hupp, J. T.; Li, S. Synthesis and optical properties of "branched" gold nanocrystals. *Nano Lett.* **2004**, *4*, 327−330.
(54) Yuan, H.; Khoury, C. G.; Hwang, H.; Wilson, C. M.; Grant, G. A.; Vo-Dinh, T. Gold nanostars: surfactant-free synthesis, 3D modelling, and two-photon photoluminescence imaging. *Nanotechnology* **2012**, *23*, 75102.
(55) Senthil Kumar, P.; Pastoriza-Santos, I.; Rodríguez-González, B.; Javier García de Abajo, F.; Liz-Marzán, L. M. High-yield synthesis and optical response of gold nanostars. *Nanotechnology* **2007**, *19*, 15606.
(56) Liz-Marzán, L. M. Tailoring surface plasmons through the morphology and assembly of metal nanoparticles. *Langmuir* **2006**, *22*, 32−41.
(57) Reguera, J.; Langer, J.; Jiménez de Aberasturi, D.; Liz-Marzán, L. M. Anisotropic metal nanoparticles for surface enhanced Raman scattering. *Chem. Soc. Rev.* **2017**, *46*, 3866−3885.
(58) Kim, W.; Kim, N.; Park, J. W.; Kim, Z. H. Nanostar probes for tip-enhanced spectroscopy. *Nanoscale* **2016**, *8*, 987−994.
(59) Cheng, L.-C.; Huang, J.-H.; Chen, H. M.; Lai, T.-C.; Yang, K.-Y.; Liu, R.-S.; Hsiao, M.; Chen, C.-H.; Her, L.-J.; Tsai, D. P. Seedless, silver-induced synthesis of star-shaped gold/silver bimetallic nanoparticles as high efficiency photothermal therapy reagent. *J. Mater. Chem.* **2012**, *22*, 2244−2253.
(60) Rothschild, W. G. Binding of hydrogen donors by peptide groups of lactams. Identity of the interaction sites. *JACS* **1972**, *94*, 8676−8683.
(61) Kan, C.; Cai, W.; Li, C.; Zhang, L. Optical studies of polyvinylpyrrolidone reduction effect on free and complex metal ions. *J. Mater. Res.* **2005**, *20*, 320−324.
(62) Zhao, Q.; Xia, Z.; Qian, T.; Rong, X.; Zhang, M.; Dong, Y.; Chen, J.; Ning, H.; Li, Z.; Hu, H.; Wu, M. PVP-assisted synthesis of ultrafine transition metal oxides encapsulated in nitrogen-doped carbon nanofibers as robust and flexible anodes for sodium-ion batteries. *Carbon* **2021**, *174*, 325.
(63) Jiang, P.; Li, S.-Y.; Xie, S.-S.; Gao, Y.; Song, L. Machinable long PVP-stabilized silver nanowires. *Chem.—Eur. J.* **2004**, *10*, 4817−4821.
(64) Schmidbaur, H.; Schier, A. Aurophilic interactions as a subject of current research: an up-date. *Chem. Soc. Rev.* **2012**, *41*, 370−412.
(65) Belloni, J.; Marignier, J.-L.; Mostafavi, M. Mechanisms of metal nanoparticles nucleation and growth studied by radiolysis. *Radiat. Phys. Chem.* **2020**, *169*, 107952.
(66) Pukies, J.; Roebke, W.; Henglein, A. Pulse-radiolytic investigation of some elementary processes of silver reduction. *Ber. Bunsen-Ges. Phys. Chem.* **1968**, *72*, 842−847.
(67) Janata, E. Early stages in the growth of small silver clusters in aqueous solution. *Radiat. Phys. Chem.* **2012**, *81*, 1404−1406.
(68) Koczkur, K. M.; Mourdikoudis, S.; Polavarapu, L.; Skrabalak, S. E. Polyvinylpyrrolidone (PVP) in nanoparticle synthesis. *Dalton Trans.* **2015**, *44*, 17883−17905.
(69) Tsuji, M.; Hashimoto, M.; Nishizawa, Y.; Kubokawa, M.; Tsuji, T. Microwave-Assisted Synthesis of Metallic Nanostructures in Solution. *Chem.—Eur. J.* **2005**, *11*, 440.
(70) José-Yacamán, M.; Miki-Yoshida, M.; Tehuacanero, S.; Zorrilla, C. On the crystal structure of nanosized gold particles. *Nanostruct. Mater.* **1994**, *4*, 61.
(71) Linek, J.; Wichterle, I.; Marsh, K. N. Vapor−Liquid Equilibria for N-Methyl-2-pyrrolidone + Benzene, +Toluene, +Heptane, and +Methylcyclohexane. *J. Chem. Eng. Data* **1996**, *41*, 1212−1218.
(72) Graf, C.; Vossen, D. L. J.; Imhof, A.; van Blaaderen, A. A General Method To Coat Colloidal Particles with Silica. *Langmuir* **2003**, *19*, 6693−6700.

https://doi.org/10.1021/acsomega.1c06835
ACS Omega 2022, 7, 9484−9495

(73) Olmon, R. L.; Slovick, B.; Johnson, T. W.; Shelton, D.; Oh, S.-H.; Boreman, G. D.; Raschke, M. B. Optical dielectric function of gold. *Phys. Rev. B: Condens. Matter Mater. Phys.* **2012**, *86*, 235147.

https://doi.org/10.1021/acsomega.1c06835
ACS Omega 2022, 7, 9484−9495